Preparation of $PbTiO_3$ nanosheets by two-step hydrothermal method with ammonia as pH-adjusting agent

JIANGLAI YUE[a], ZHIXIONG HUANG[a], DONGYUN GUO[a,*], YANG JU[b]
[a]*School of Materials Science and Engineering, Wuhan University of Technology, Wuhan 430070, China*
[b]*Department of Mechanical Science and Engineering, Nagoya University, Nagoya 464-8603, Japan*

The $PbTiO_3$ nanocrystals were synthesized by a two-step hydrothermal method, and ammonia solution was used as a pH-adjusting agent. The effect of ammonia concentration in the second-step Pb-Ti precursors on crystallization and morphologies of $PbTiO_3$ nanocrystals was investigated. The single-phase $PbTiO_3$ nanocrystals were formed by the two-step hydrothermal method at 200 ^oC for 20 h. As the ammonia concentration in the second-step Pb-Ti precursor ranged from 4.4 to 8.8 mol/L, the single-crystal $PbTiO_3$ nanosheets with thickness of about 45 nm were synthesized, and a few rectangular nanocrystals were also observed. The ferroelectric domains were observed in the $PbTiO_3$ nanocrystals prepared at the ammonia concentration of 4.4 mol/L, which indicated that the $PbTiO_3$ nanocrystals with ferroelectric behavior were formed.

(Received February 23, 2021; accepted October 7, 2021)

Keywords: $PbTiO_3$ nanocrystal, Two-step hydrothermal method, Ammonia solution, Morphology, Ferroelectric domain

1. Introduction

As a typical perovskite oxide, lead titanate ($PbTiO_3$) is one of the important members in the ferroelectric families with a high Curie temperature of 490 ^oC, which has been widely applied in microelectronic devices [1-6]. To meet the increasing demand for device miniaturization, varied $PbTiO_3$ nanostructures have been synthesized by various techniques, such as solid-state reaction, co-precipitation, sol-gel, and hydrothermal methods, etc. [7-17]. Among these methods, hydrothermal method has been extensively applied in preparation of $PbTiO_3$ nanocrystals, which can control over the nucleation and crystal growth by varying the reaction conditions [10-17].

Li et al. [10] synthesized $PbTiO_3$ particles by hydrothermal method, and NaOH was chosen as the pH-adjusting agent. Recently, Xu et al. [11] synthesized single-crystalline tetragonal perovskite $PbTiO_3$ nanosheets via hydrothermal method by employing $K_2Ti_6O_{13}$ nanofibers as titanium sources with the pH-adjusting agent of KOH. Abirami et al. [12] synthesized $PbTiO_3$ nanoparticles by hydrothermal method at 200 ^oC for 18 h. In this process, $Pb(NO_3)_2$, titanium isoproxide and NaOH were used as starting materials. Yuan et al. [13] also employed $K_2Ti_6O_{13}$ as the precursor to synthesize the PX-$PbTiO_3$ nanowires. In these cases, KOH or NaOH was chosen as the pH-adjusting agent. However, the alkalis introduced the undesirable impurities to $PbTiO_3$ nanocrystals. Bao et al. [14] and Cho et al. [15] synthesized $PbTiO_3$ particles by hydrothermal method with an alkali-free pH-adjusting agent of tetramethylammonium hydroxide (TMAH) to avoid the contamination of alkalis. However, TMAH is quite expensive with strong corrosive and toxic properties. The ammonia aqueous solution is also a kind of alkali-free pH-adjusting agents. In our previous study, the dendritic $PbTiO_3$ nanorods were synthesized by an eco-friendly hydrothermal method with ammonia as the pH-adjusting agent [16, 17]. However, only irregular dendritic $PbTiO_3$ nanorods were synthesized due to the weak base of ammonia solution. To obtain $PbTiO_3$ nanocrystals with well crystallization, the two-step hydrothermal method was adopted to prepare the $PbTiO_3$ nanocrystals. The effect of ammonia concentration in the second-step Pb-Ti precursors on crystallization of $PbTiO_3$ nanocrystals was investigated, and the ferroelectric domains of $PbTiO_3$ nanocrystals were analyzed using piezoresponse force microscopy (PFM) technique.

2. Experimental details

All the reagents were of analytical grade purity and were used without further purification. Lead acetate

trihydrate ($(Pb(CH_3COO)_2 \cdot 3H_2O$), bis(ammonium lactate) titanium dihydroxide ($C_6H_{18}N_2O_8Ti$) and ammonia solution were used as the starting materials. The desired amounts of $Pb(CH_3COO)_2 \cdot 3H_2O$ and $C_6H_{18}N_2O_8Ti$ were dissolved in deionized water, and stirred at room temperature to form the first-step Pb-Ti precursors. And then, the ammonia solution was added to the first-step Pb-Ti precursors with stirring, the nominal Pb-Ti concentration was 0.05 mol/L, the nominal ammonia concentration was about 8.8 mol/L, and the precipitates were formed. The precipitates were centrifuged and washed with deionized water. Finally, the precipitates were dispersed in the deionized water to form the second-step Pb-Ti precursors at different nominal ammonia concentrations (0, 4.4 and 8.8 mol/L). The 30 ml resulting suspensions were added to Teflon-lined autoclaves of 50 ml capacity, and they were sealed tightly. The autoclaves were heated at 200 ^oC for 20 h, and then naturally cooled to room temperature. The precipitates were centrifuged and washed with deionized water and ethanol in sequence. The $PbTiO_3$ nanocrystals were dispersed in ethanol to form a suspended solution, and then the suspended solution was dropped on a platinized silicon substrate. After the ethanol solvent was volatile, only the $PbTiO_3$ nanocrystals were left on the substrate for the ferroelectric domain measurement using PFM.

The X-ray diffraction patterns of these samples were analyzed by an X-ray diffractometer (XRD, D/MAX-RB) with Cu*Kα* radiation (40 kV, 30 mA). The scanning rate was 2 ^{o}/min with scanning step of 0.02^o. The morphologies of these samples were characterized by a field emission scanning electron microscope (FESEM, JSM-7500F). The $PbTiO_3$ nanosheet was analyzed by a high-resolution transmission electron microscopy (HR-TEM, JEM-2100F). The ferroelectric domain of the $PbTiO_3$ nanocrystals was investigated with the PFM (Nanoscope IV).

3. Results and discussion

The XRD results of these precipitates prepared at different ammonia concentrations in the second-step Pb-Ti precursors are shown in Fig. 1. The XRD patterns were indexed according to JCPDS card No. 78-0298 (tetragonal $PbTiO_3$ phase with space group P4 mm). All precipitates showed the clear and sharp diffraction peaks of tetragonal $PbTiO_3$ phase, which indicated that the pervoskite $PbTiO_3$ phase was formed. As the ammonia concentration increased from 0 to 4.4 mol/L in the second-step Pb-Ti precursors, the intensity of diffraction peaks obviously increased. With continuous increase of the ammonia concentration from 4.4 to 8.8 mol/L, there was no obvious change of the XRD patterns.

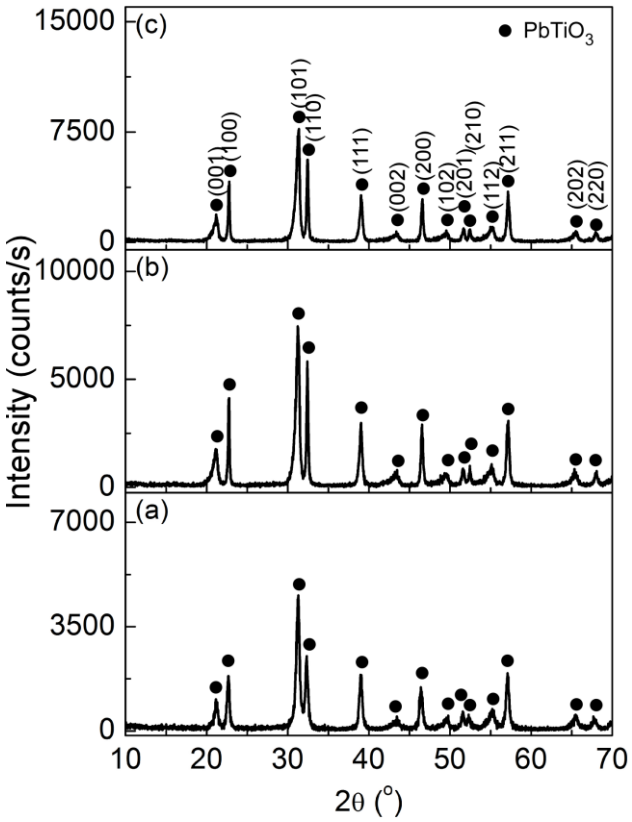

Fig. 1. XRD patterns of the samples prepared at different ammonia concentrations in the second-step Pb-Ti precursors: (a) 0, (b) 4.4 mol/L and (c) 8.8 mol/L

Fig. 2 displays the morphologies of these $PbTiO_3$ precipitates prepared at different ammonia concentration in the second-step Pb-Ti precursors. When the $PbTiO_3$ precipitate was prepared without ammonia in the second-step Pb-Ti precursor, the $PbTiO_3$ nanocrystals showed irregular morphologies. As the precipitates were synthesized at the ammonia concentration of 4.4 and 8.8 mol/L, the precipitates mainly consisted of nanosheets, and a few rectangular nanocrystals were also observed. The thickness of $PbTiO_3$ nanosheets was about 45 nm, and the edge of $PbTiO_3$ nanosheets was coarse. The ammonia reacted with water to produce $(NH_4)^+$ and OH^- ions in the aqueous solution. In the first-step Pb-Ti precursors, the Pb^{2+} and Ti^{4+} ions reacted with OH^- ions to form the mixture precipitates of $Pb(OH)_2$ and $Ti(OH)_4$. In the second-step Pb-Ti precursors, the mixture precipitates of $Pb(OH)_2$ and $Ti(OH)_4$ could form $PbTiO_3$ nanocrystals under hydrothermal conditions without ammonia. However, since the OH^- ions were not enough for the growth of $PbTiO_3$ nanocrystals, only tiny $PbTiO_3$ nanocrystals were formed. When the $PbTiO_3$ precipitates were synthesized at ammonia concentration of 4.4 mol/L, the ammonia could supply enough OH^- ions for the growth of $PbTiO_3$ nanocrystals, and $PbTiO_3$ nanosheets with well crystallization were formed. When the ammonia reacted

with water to form $(NH_4)^+$ and OH^- ions, the reaction was reversible, and almost 99% of the ammonia existed as ammonia molecules. As the ammonia concentration increased from 4.4 to 8.8 mol/L, there was no obvious change in the OH^- concentration. Then the similar XRD patterns and morphologies of the $PbTiO_3$ precipitates prepared at ammonia concentration of 4.4 to 8.8 mol/L were observed.

Fig. 3 shows the typical TEM images and the corresponding selected area electron diffraction (SAED) pattern of $PbTiO_3$ nanosheet prepared at ammonia concentration of 4.4 mol/L in the second-step Pb-Ti precursor. A typical rectangular nanosheet was observed, and the lateral size of the nanosheet was about 200 nm, as shown in Fig. 3(a). The dotted area in Fig. 3(a) is enlarged and shown in Fig. 3(b). The high-resolution TEM image indicated that the two sets of lattice fringes with interplanar intervals of 0.3892 nm agreed well with the spacing of the (100) and (010) planes of tetragonal $PbTiO_3$ phase (JCPDS card No. 78-0298). Its corresponding SAED pattern is shown in Fig. 3(c). According to the tetragonal $PbTiO_3$ phase, the theoretical angles between the (010) and (100) planes, (110) and (100) planes were 90^o and 45^o, respectively. The measured angles between the (010) and (100) planes, (110) and (100) planes were 90.12^o and 45.09^o, respectively, as shown in Figs. 3 (b) and (c). The measured angles were very close to the theoretical angles, which confirmed that the single-crystal $PbTiO_3$ nanosheet was prepared.

The ferroelectric domains of the $PbTiO_3$ nanocrystals deposited on $Pt/Ti/SiO_2/Si$ substrate were characterized by applying 6 V AC to a metal-coated tip at 15 kHz. Fig. 4 displays the morphology image and phase for the same region (1×1 μm^2) of piezoresponse signal of $PbTiO_3$ nanocrystals prepared at ammonia concentration of 4.4 mol/L. Ferroelectric domains had the same dimension as the $PbTiO_3$ nanocrystals, which indicated that one ferroelectric domain corresponded to one $PbTiO_3$ nanocrystal [18-20]. In the next research, further investigation for the piezoresponse of $PbTiO_3$ nanosheets should be done.

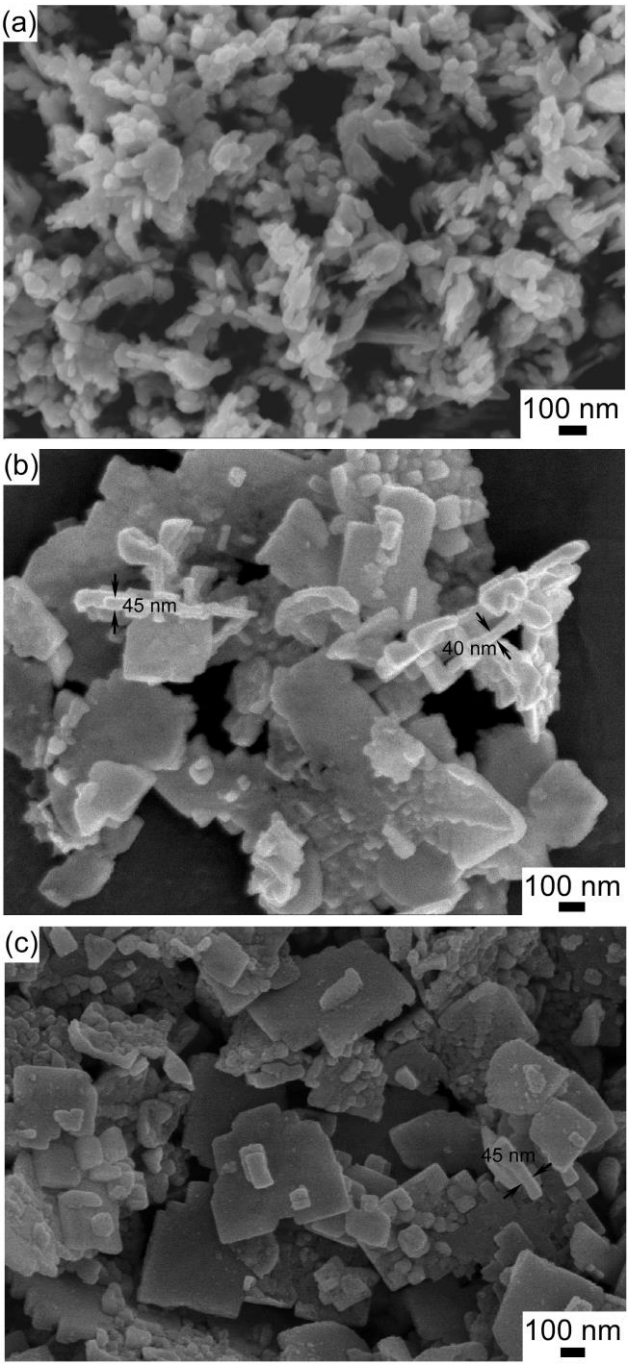

Fig. 2. Morphologies of the $PbTiO_3$ nanocrystals prepared at different ammonia concentrations in the second-step Pb-Ti precursors: (a) 0, (b) 4.4 mol/L and (c) 8.8 mol/L

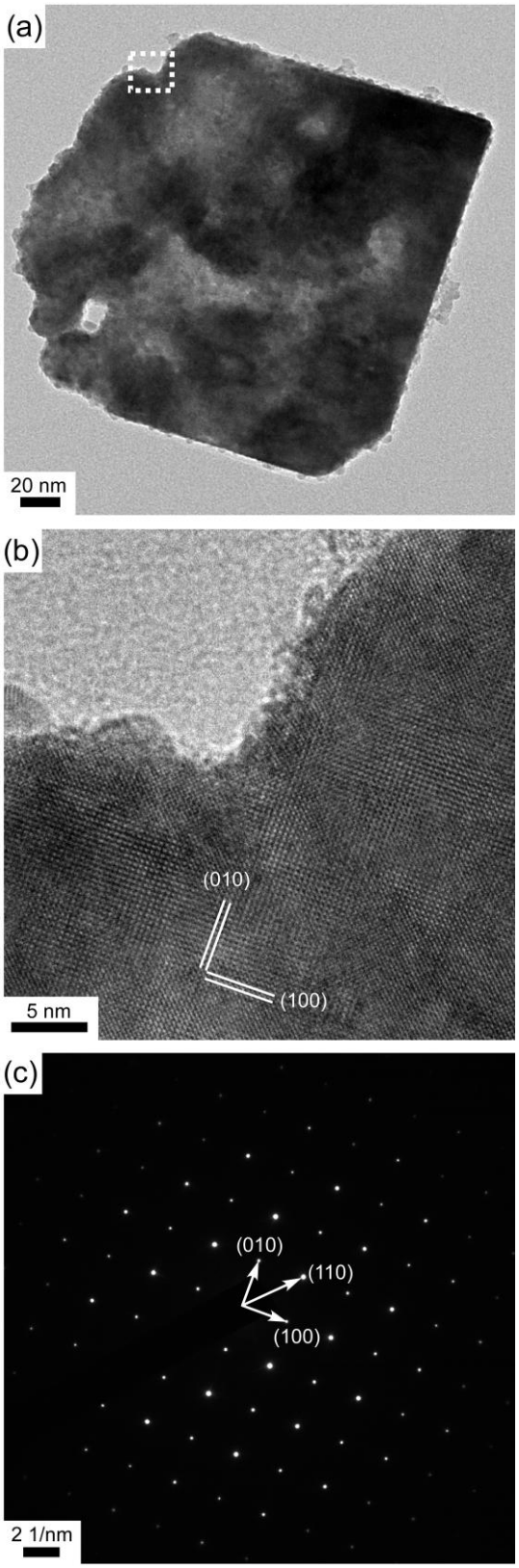

Fig. 3. TEM image (a) of $PbTiO_3$ nanosheet prepared at ammonia concentration of 4.4 mol/L in the second-step Pb-Ti precursor, high-resolution TEM image (b) of the dash-line area of (a) and its corresponding selected area electron diffraction (SAED) pattern (c)

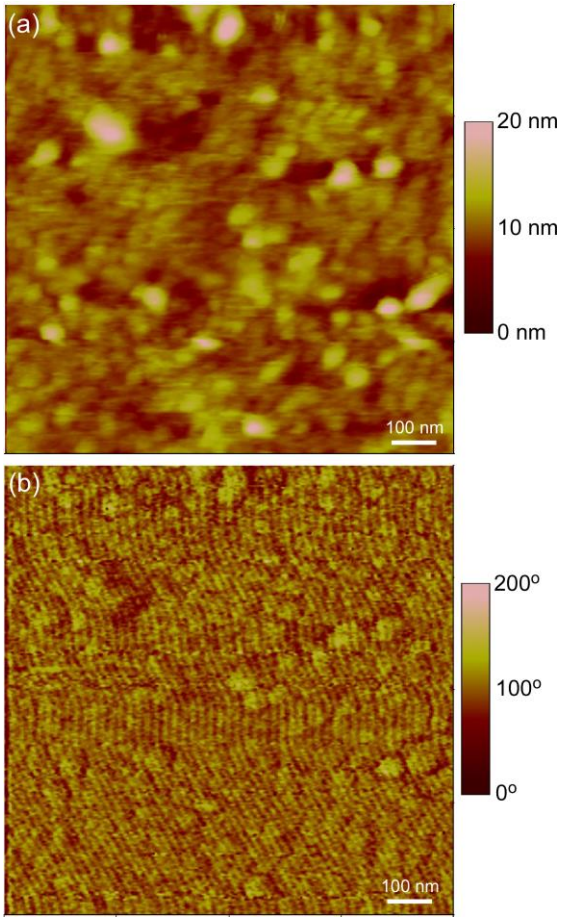

Fig. 4. Morphology image (a) and phase (b) for the same region of piezoresponse signal of $PbTiO_3$ nanocrystals deposited on $Pt/Ti/SiO_2/Si$ substrate at ammonia concentration of 4.4 mol/L in the second-step Pb-Ti precursor (color online)

4. Conclusion

The single-phase $PbTiO_3$ nanocrystals were synthesized by the two-step hydrothermal method with the pH-adjusting agent of ammonia solution. When the ammonia concentration in the second-step Pb-Ti precursor ranged from 4.4 to 8.8 mol/L, the single-crystal $PbTiO_3$ nanosheets with thickness of about 45 nm were synthesized, and a few rectangular nanocrystals were also observed. The ferroelectric domains were observed in the $PbTiO_3$ nanocrystals, which indicated that the ferroelectric $PbTiO_3$ nanocrystals were formed.

Acknowledgement

This work was supported by the National Natural Science Foundation of China (Grant No. 51272195).

References

[1] T. Shimada, T. Xu, Y. Araki, J. Wang, T. Kitamura, Nano Lett. **17**, 2674 (2017).
[2] Y. Feng, Y. Tang, Y. Zhu, M. Zou, Y. Wang, X. Ma, J. Appl. Phys. **128**, 224102 (2020).
[3] M. F. Sarott, M. Fiebig, M. Transsin, Appl. Phys. Lett. **117**, 132901 (2020).
[4] R. Nishino, T. C. Fujita, F. Kagawa, M. Kawasaki, Sci. Rep. **10**, 10864 (2020).
[5] Y. Feng, M. Xu, H. Liu, W. Li, H. Li, Z. Bian, Nano Energy **73**, 104768 (2020).
[6] G. Liu, L. Kong, Q. Hu, S. Zhang, Appl. Phys. Rev. **7**, 021405 (2020).
[7] R. Wongmaneerung, S. Choopan, R. Yimnirun, S. Ananta, J. Alloy. Compd. **509**, 3547 (2011).
[8] S. Dhage, Y. Khollam, H. Potdar, S. Deshpande, B. Sarwade, S. Date, Mater. Lett. **56**, 564 (2002).
[9] R. Bel-Hadj-Tahar, M. Abboud, Solid State Sci. **78**, 74 (2018).
[10] Y. Li, H. Sun, N. Wang, W. Fang, Z. Li, Solid State Sci. **37**, 18 (2014).
[11] G. Xu, X. Huang, V. Krstic, S. Chen, X. Yang, C. Chao, G. Shen, G. Han, CrystEngComm **16**, 4373 (2014).
[12] R. Abirami, T. Senthil, S. Kalpana, L. Kungumadevi, M. Kang, Mater. Lett. **279**, 128507 (2020).
[13] S. Yuan, B. Li, J. Wang, J. Cryst. Growth **546**, 125792 (2020).
[14] L. Bao, J. He, G. Xu, Y. Zhao, X. Yang, G. Shen, G. Han, Chinese J. Chem. **35**, 1043 (2017).
[15] S. Cho, J. Noh, M. M. Lencka, R. E. Riman, J. Eur. Ceram. Soc. **23**, 2323 (2003).
[16] X. Li, Z. Huang, L. Zhang, D. Guo, Mater. Lett. **14**, 610 (2018).
[17] X. Li, J. Yue, Z. Huang, L. Zhang, D. Guo, Y. Ju, J. Mater. Sci. Mater. Electron. **31**, 12345 (2020).
[18] A. Gruverman, S. V. Kalinin, J. Mater. Sci. **41**, 107 (2006).
[19] A. Lipatov, T. Li, N. S. Vorobeva, A. Sinitskii, A. Gruverman, Nano Lett. **19**, 3194 (2019).
[20] J. G. M. Guy, L. Zhang, J. Chen, J. M. Gregg, J. F. Scott, Appl. Phys. Lett. **116**, 182903 (2020).

*Corresponding author: guody@whut.edu.cn